Check for updates

ADVANCED FUNCTIONAL MATERIALS
www.afm-journal.de

Ultra-Effective Light-Activated Antibacterial Activity via Carboxyl Functionalized Graphene Quantum Dots and Films

Muhammad Hassnain, Laure S. van Hofwegen, Humeyra Nur Kaleli, Temirlan Kubanaliev, Zafer Eroglu, Asim Onal, Payal P. S. Balraadjsing, Onder Metin, Fahri Alkan, Sebastian A. J. Zaat, and Sedat Nizamoglu**

Bacterial infections are a major healthcare concern. Clinical application of photo-activated quantum dots to efficiently treat bacterial infections has been hindered by inadequate production of reactive oxygen species. In this study, photoactive antimicrobial carboxyl-functionalized graphene quantum dots (cGQDs) are synthesized with an exceptionally high singlet oxygen ($^1O_2$) quantum yield of 0.88. Compared to non-functionalized GQDs, cGQDs exhibit over a 20-fold enhancement in the $^1O_2$ quantum yield. According to the density functional theory simulations, the dramatic increase of $^1O_2$ quantum yield is due to significantly enhanced spin–orbit coupling between singlet and triplet excited states of GQDs with addition of —COOH groups. Under low-intensity blue light (5 mW cm^{-2}), *Staphylococcus aureus* is completely eliminated with just 0.8 µg mL^{-1} of cGQDs, and a minimum bactericidal concentration (MBC) of 0.4 µg mL^{-1} is determined, representing the lowest MBC reported against *S. aureus* using light-activated quantum dots. Layer-by-layer assembly of cGQD films also results in over a 99.9% reduction against multi-drug resistant *Staphylococcus aureus* and *Escherichia coli* under illumination. cGQDs, both in suspension and as a nano-assembled film, exhibit good cell viability in mammalian cells under both dark and light conditions. These results highlight the strong potential of cGQDs as an effective nanomaterial for antibacterial applications.

1. Introduction

The treatment of bacterial infections and associated diseases has been identified as being one of the most challenging health-related problems for several decades.[1–3] The World Health Organization (WHO) through a report in 2014[4] and follow-up implementation reports[5,6] categorically warned about the impending "post-antibiotic" era, where even minor injuries and ordinary bacterial infections may prove fatal. This phenomenon is a direct consequence of the growing prevalence of antibiotic resistance among bacteria.[7,8] Therefore, there is a growing need for alternative prevention and treatment strategies against bacterial infection.[9,10] Among the developed strategies, antibacterial photodynamic therapy (APDT) is a promising alternative approach using the combination of a photosensitizer, light and oxygen to generate reactive oxygen species (ROS) that damage and kill bacterial cells.[11–14]

Semiconductor quantum dots (QDs) have emerged as a promising class of

M. Hassnain, A. Onal, S. Nizamoglu
Department of Biomedical Science and Engineering
Koç University
Istanbul 34450, Türkiye
E-mail: snizamoglu@ku.edu.tr

L. S. van Hofwegen, P. P. S. Balraadjsing, S. A. J. Zaat
Department of Medical Microbiology and Infection Prevention
Amsterdam institute for Immunology and Infectious Diseases
Amsterdam UMC
University of Amsterdam
Meibergdreef 9, Amsterdam 1105 AZ, The Netherlands
E-mail: s.a.zaat@amsterdamumc.nl

The ORCID identification number(s) for the author(s) of this article can be found under https://doi.org/10.1002/adfm.202421537

© 2025 The Author(s). Advanced Functional Materials published by Wiley-VCH GmbH. This is an open access article under the terms of the Creative Commons Attribution-NonCommercial-NoDerivs License, which permits use and distribution in any medium, provided the original work is properly cited, the use is non-commercial and no modifications or adaptations are made.

DOI: 10.1002/adfm.202421537

H. N. Kaleli
Research Center for Translational Medicine (KUTTAM)
Koç University
Istanbul 34450, Türkiye

T. Kubanaliev, Z. Eroglu, O. Metin
Department of Chemistry
Koç University
Istanbul 34450, Türkiye

O. Metin
Koç University Surface Science and Technology Center (KUYTAM)
Istanbul 34450, Türkiye

F. Alkan
Department of Chemistry
Bilkent University
Ankara 06800, Türkiye

S. Nizamoglu
Department of Electrical and Electronics Engineering
Koç University
Istanbul 34450, Türkiye

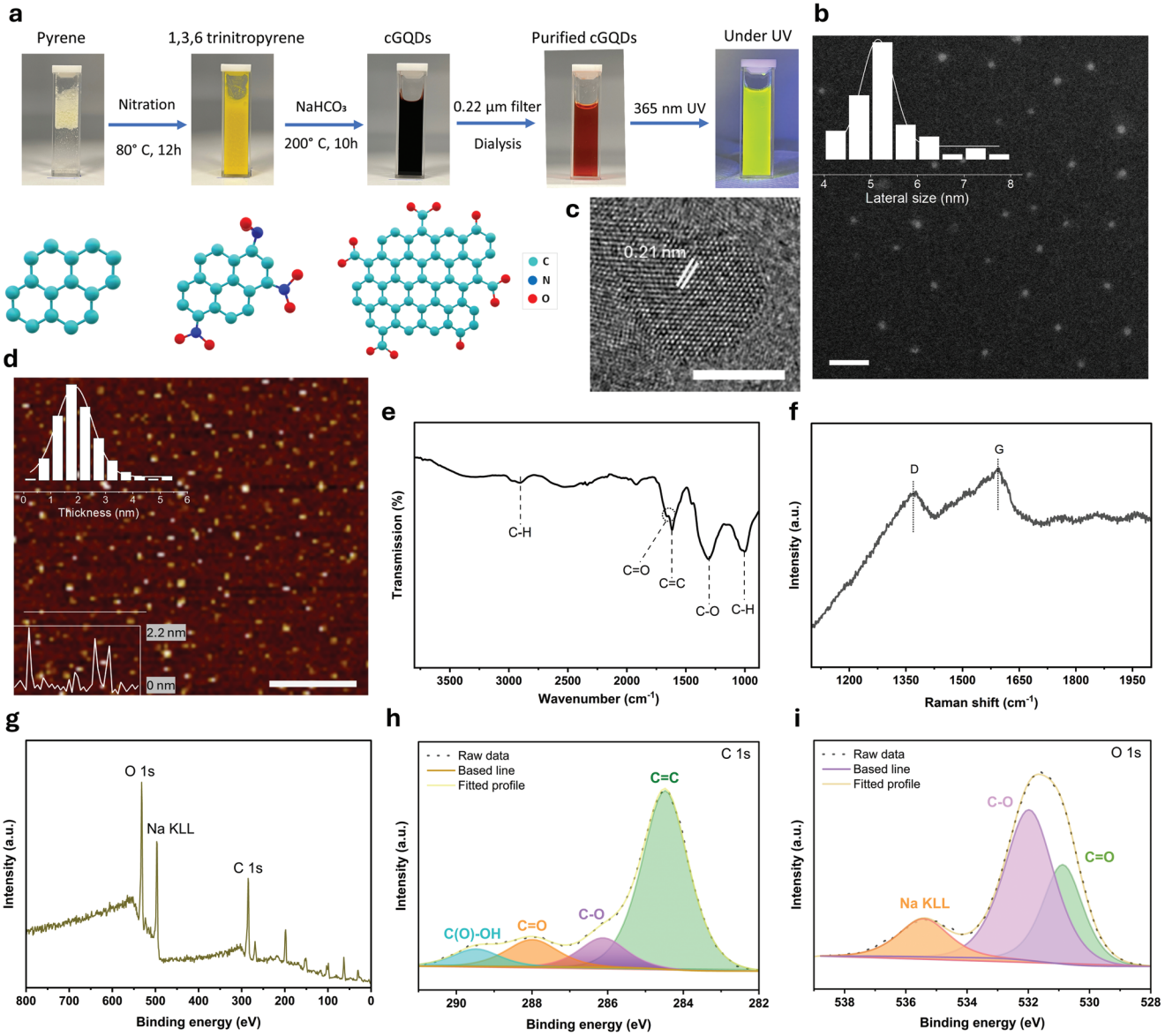

Figure 1. Synthesis and structural characterization of cGQDs. a) The synthesis route of cGQDs and structure diagram of the synthesis process. b) STEM image, scale bar: 40 nm (inset: lateral size distribution). c) HRTEM image, scale bar: 5 nm. d) AFM image (insets: histogram of thickness profile and height distribution over the indicated white line). Scale bar: 1 μm. e) FTIR spectrum of the dried cGQDs. f) Raman spectrum under 633 nm laser excitation. g) XPS survey spectrum. h) Deconvolution of high resolution C 1s spectrum. i) Deconvolution of high resolution O 1s spectrum.

photosensitizers for potential use in APDT, owing to their ability to induce ROS-mediated bacterial killing upon light exposure.[15,16] The clinical translation of inorganic quantum dots has been hindered by their cytotoxicity, which may result from the release of heavy metals such as cadmium or lead, limited water solubility, and inefficient ROS generation.[17] Carbon-based QDs, especially graphene quantum dots (GQDs) are preferred over inorganic QDs owing to their biocompatibility,[18,19] excellent solubility in water and other solvents such as ethanol, DMF, DMSO,[20] good photo-stability,[21] and easy and cheap synthesis procedure.[22] GQDs are 0D semiconductor nanocrystals composed of 1–5 layers of sp^2 hybridized carbon atoms arranged in a hexagonal lattice.[23–26] Their optoelectronic properties can be varied via doping,[27] size tunability,[28] and various surface functional groups.[29–31] Moreover, their small lateral size (2–10 nm) and ultrathin structure (≈1 nm) leads to a high specific surface area, which enables easier penetration and localization within bacterial cells and results in a more effective bactericidal effect.[32,33]

Previous studies have shown that GQDs and their derivatives (modified through doping and functionalization methods) can generate ROS upon photoactivation, making them suitable for antibacterial applications.[34–36] For example, nitrogen-doped GQDs showed antimicrobial activity against gram-negative *Escherichia coli* due to generation of singlet oxygen ($^1O_2$) under red light illumination (100 mW cm^{-2}).[37] Recently, it was

© 2025 The Author(s). Advanced Functional Materials published by Wiley-VCH GmbH

16163028, 2025, 26, Downloaded from https://advanced.onlinelibrary.wiley.com/doi/10.1002/adfm.202421537 by Koc University, Wiley Online Library on [02/09/2025]. See the Terms and Conditions (https://onlinelibrary.wiley.com/terms-and-conditions) on Wiley Online Library for rules of use; OA articles are governed by the applicable Creative Commons License

reported that L-cysteine-modified GQDs generate $^1O_2$ upon blue light illumination (3 W), which is known to have bactericidal activity against *Staphylococcus aureus*, *Enterococcus faecalis*, and *Escherichia coli*.[38] However, the findings revealed limited bactericidal effectiveness of these GQDs, even under high-intensity light exposure for long time periods, due to insufficient quantum yield of ROS produced. Moreover, these GQDs were only tested in solution, but since the presence of an inserted or implanted device increases susceptibility to infection,[39,40] there is also an urgent need for stable and highly efficient ROS-producing GQD thin films. Particularly devices continuously exposed to the patient's microflora, such as dental implants, transcutaneous catheters, and wound dressings are among applications that are at risk for infection and could majorly benefit from a bactericidal implant coating.

To overcome these limitations, we present synthesis of carboxyl-functionalized graphene quantum dots (cGQDs) using a simple hydrothermal method with trinitropyrene as the carbon source. The resulting colloidal cGQDs exhibited an exceptionally high $^1O_2$ quantum yield of 0.88. Density functional theory (DFT) calculations indicate that this high $^1O_2$ quantum yield is due to enhanced spin–orbit coupling, a result of the —COOH functionalization. In suspension, the cGQDs demonstrated potent bactericidal activity against *S. aureus* and *E. coli* when exposed to blue light. Moreover, cGQDs incorporated into a novel, custom-designed coated film achieved over 99.9% reduction in bacterial inocula of both susceptible and multi-drug resistant *S. aureus* and *E. coli* under low-intensity illumination (5 mW cm^{-2}). These results highlight the potential of cGQDs, both in suspension and as medical device coatings, as a promising antibacterial agent.

2. Results and Discussion

2.1. Synthesis

Inspired by the synthesis of OH and NH_2 functionalized GQDs,[41] we synthesized cGQDs by subjecting 1,3,6-trinitropyrene to the hydrothermal treatment in an $NaHCO_3$ aqueous solution (**Figure 1a**). Polyaromatic hydrocarbons (PAH) are known for being exceptionally stable and it is difficult to convert them into graphene-like structures. Typically, a high reaction temperature over 700 °C is required for dehydrogenation. However, using the hydrothermal synthesis method at high internal pressure, it is possible to graft graphene structures out of PAH molecules at lower temperatures ranging from 120 to 250 °C.[42] Trinitropyrene was used as a starting material, which contains electron withdrawing nitro groups (NO_2), that are available for nucleophilic aromatic substitution reactions with alkaline counter ions grafting —COOH groups onto the GQD surface.

2.2. Structural Characterization

The morphology and lateral size distribution of cGQDs was analyzed using scanning transmission electron microscopy (STEM). The average lateral size of cGQDs is 5.4 ± 0.7 nm (Figure 1b) and an interplanar distance of 0.21 nm corresponds to the lattice spacing of graphene along the (001) direction (Figures 1c and S1, Supporting Information). Previous research on 1,3,6-trinitropyrene-based GQDs synthesis reported average lateral sizes of 3.5 nm for hydroxyl-functionalized GQDs and 2.8 nm for amine-functionalized GQDs, both of which are smaller than cGQDs; this increased size is attributed to carboxyl functionalization, which enhances the fusion of more trinitropyrene molecules during the hydrothermal reaction. The thickness of cGQDs analyzed by atomic force microscopy (AFM) revealed that cGQDs have an average thickness of 1.92 ± 0.6 nm (Figure 1d), corresponding to an average of 5.6 carbon atom layers. The Fourier-transform infrared spectroscopy (FTIR) spectrum (Figure 1e) of dried cGQDs showed a strong vibration at 1617 cm^{-1}, attributed for C=C bonds indicating graphitization, along with an overlapping peak at 1556 cm^{-1}, associated with C=O bonds confirming the presence of —COOH functional groups. Raman spectroscopy (Figure 1f) with a laser excitation of 633 nm further supported these findings, showing a G peak at 1589 cm^{-1} due to sp^2-hybridized carbon atoms in the GQD lattice, along with a pronounced D peak at 1376 cm^{-1} indicating high degree of disorder in the cGQD structure due to —COOH functionalization. The G-to-D intensity ratio of 1.1 suggests high level of graphitization. X-ray photoelectron spectroscopy (XPS) survey scan (Figure 1g) revealed strong signals for C 1s and O 1s along with a signal from impurity Na^+ and a negligible N1s signal at ≈400 eV. High-resolution XPS spectra showed a prominent C 1s signals at 284.8 eV for C=C bonds and 289.2 eV for C(O)—OH, confirming the presence of sp^2-hybridized carbon atoms and carboxyl groups (Figure 1h). The O 1s peaks at 531.1 eV and 532.8 eV correspond to C=O and C—O bonds, respectively (Figure 1i). These results highlight the —COOH functionalization and high graphitization in the cGQD structure, with negligible nitrogen signals indicating efficient conversion of trinitropyrene to cGQDs during synthesis.

2.3. Photophysical Characterization

The photon absorption of cGQDs in the ultraviolet and visible regions of the electromagnetic spectrum is one of their key photophysical characteristics that drives the photochemical activity (**Figure 2a**). The absorption spectrum of cGQDs showed a strong excitonic peak at 488 nm, with a shoulder peak at 463 nm (Figure 2b), originating from electron transitions between the π–π^* energy levels of the GQDs.[41] When exposed to 365 nm UV light, the cGQDs emitted a dense yellowish-green fluorescence (Figure 1a), with a photoluminescence (PL) peak at 542 nm and a Stokes shift of 54 nm (Figure 2b). cGQDs exhibited PL peaks with minor variation in the range of 532–556 nm under excitation wavelengths of 300–500 nm (Figure S2, Supporting Information). The photoluminescence quantum yield (PLQY) of the synthesized cGQDs was 5%, which is lower than the 23% for unfunctionalized GQDs (Figure S3, Supporting Information), and PLQYs over 20% have been previously reported for other functionalized GQDs.[41,43] This decreased PLQY is primarily attributed to the carboxylation process, which introduces —COOH groups to the GQD surface, increasing defects that act as non-radiative recombination centers. This feature can limit the application of cGQDs in certain biomedical applications such as bioimaging that require high fluorescence features. However,

© 2025 The Author(s). Advanced Functional Materials published by Wiley-VCH GmbH

16163028, 2025, 26, Downloaded from https://advanced.onlinelibrary.wiley.com/doi/10.1002/adfm.202421537 by Koc University, Wiley Online Library on [02/09/2025]. See the Terms and Conditions (https://onlinelibrary.wiley.com/terms-and-conditions) on Wiley Online Library for rules of use; OA articles are governed by the applicable Creative Commons License

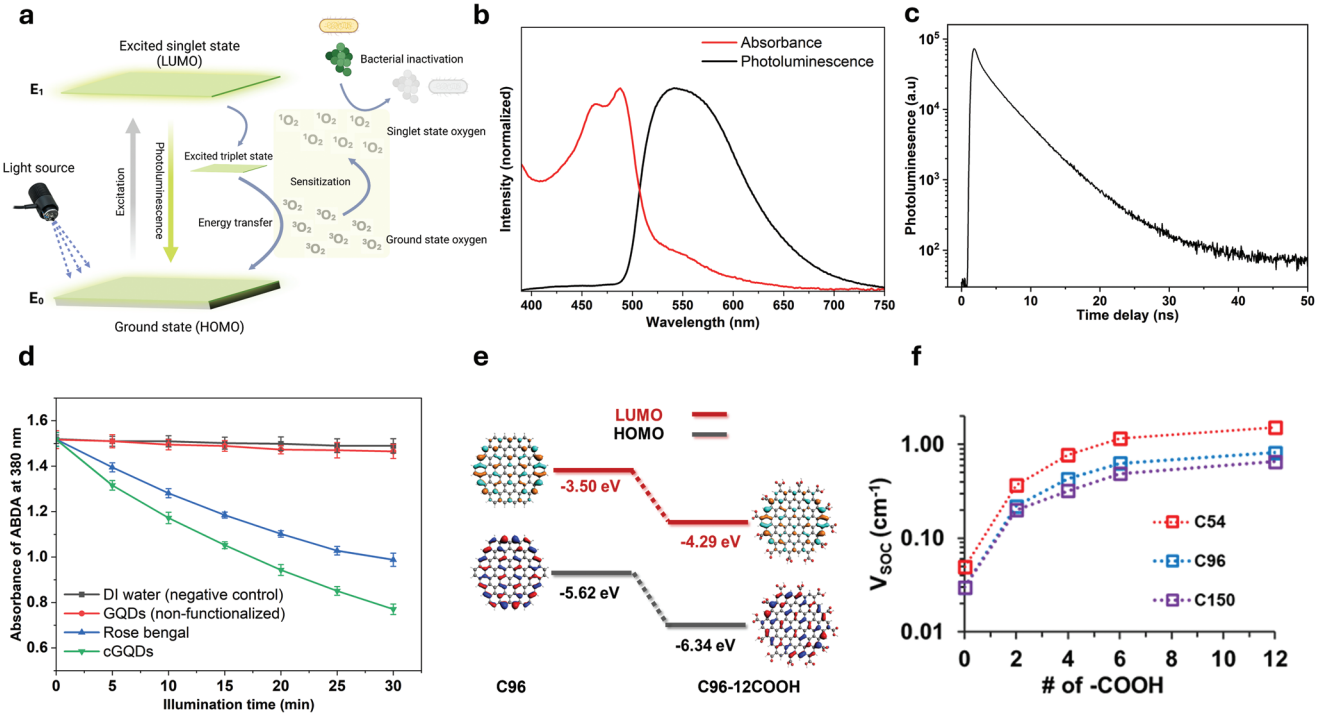

Figure 2. Photophysical/photochemical characterization of cGQDs and DFT simulation. a) Schematic illustration of photoexcitation/photoluminescence, spin–orbit coupling (intersystem crossing), singlet oxygen formation, and antimicrobial mechanism of cGQDs. b) UV–Vis absorption and emission spectra of cGQDs. c) Time-resolved fluorescence decay of cGQDs recorded at 542 nm. d) Photodegradation of ABDA single oxygen probe due to formation of $^1O_2$ in presence of DI water (negative control), non-functionalized GQDs, rose bengal, and cGQDs. e) Theoretical results for the model GQD systems using DFT with B3LYP/DZP level of theory for Illustration of HOMO and LUMO levels and the alteration in their energies upon functionalization with —COOH. f) Calculated spin–orbit coupling matrix elements (V_{SOC}) between T_1 and S_1 states as a function of —COOH functionalization.

lower PLQY yet efficient intersystem crossing of the paired electrons from the singlet excited state to the triplet exited state is highly desirable for efficient ROS generation. Moreover, the time-resolved PL spectrum of cGQDs (Figure 2c) revealed a photoluminescence decay with a lifetime of 3.4 ns where a fluorescence lifetime at the nanosecond level implies the singlet state characteristic of emission.

2.4. Photochemical Characterization

To evaluate and quantify singlet oxygen ($^1O_2$) formation in cGQDs, 9,10-anthracenediyl-bis(methylene)dimalonic acid (ABDA) was used as a sensor probe. ABDA quickly decomposes after chemically reacting irreversibly with $^1O_2$ resulting in decrease of its absorbance as an indication of $^1O_2$ formation.[44–46] Absorption intensity of ABDA significantly decreased in the cGQD solutions, indicating high concentration of $^1O_2$ produced upon blue light illumination (Figures 2d and S5b, Supporting Information). Comparatively, lesser photodegradation of ABDA probe was observed with standard photosensitizer RB as compared to cGQDs indicating that the $^1O_2$ production of cGQD is higher than RB (Figures 2d and S5e, Supporting Information). We characterized the $^1O_2$ quantum yield (QY) and while RB has a typical $^1O_2$-QY of 0.75 in water,[17] cGQDs showed a relatively higher $^1O_2$-QY value of 0.88. Moreover, non-functionalized GQDs showed minimal degradation of ABDA corresponding to a low $^1O_2$-QY of 0.045 (Figure S5c, Supporting Information) which corresponds to 20-fold lower $^1O_2$-QY as compared to cGQDs. To detect superoxide anion radical ($O_2^{\bullet-}$), XTT assay (sodium 3′-[1- (phenylaminocarbonyl)- 3,4- tetrazolium]-bis (4-methoxy6-nitro) benzene sulfonic acid hydrate) was used.[47] However, no increase was observed in the absorption peak of XTT at 470 nm upon blue light illumination, indicating absence of superoxide anion in the medium (Figure S6, Supporting Information).

2.5. Density Functional Theory Calculation

To understand the exceptional $^1O_2$-QY of cGQDs, we performed density functional theory (DFT) calculations employing the B3LYP/DZP level of theory (see computational methods for details). Three models of GQDs (C54, C96, and C150) were employed for the computations (Figure S7a, Supporting Information). For each model system, —COOH functionalization was assessed with 2, 4 6, and 12 —COOH units (Figure S7b, Supporting Information). In general, the calculated excited states exhibited a slight redshift with increasing —COOH functionalization as evident from the theoretical spectra of C50 (Figure S8a, Supporting Information), C96 (Figure S8c, Supporting Information), and C150 (Figure S8e, Supporting Information). Meanwhile, both highest occupied molecular orbital (HOMO) and lowest

© 2025 The Author(s). Advanced Functional Materials published by Wiley-VCH GmbH

16163028, 2025, 26, Downloaded from https://advanced.onlinelibrary.wiley.com/doi/10.1002/adfm.202421537 by Koc University, Wiley Online Library on [02/09/2025]. See the Terms and Conditions (https://onlinelibrary.wiley.com/terms-and-conditions) on Wiley Online Library for rules of use; OA articles are governed by the applicable Creative Commons License

unoccupied molecular orbital (LUMO) energies showed significant stabilization with —COOH functionalization as a result of combined mesomeric and inductive effects (Figure 2e and Table S3, Supporting Information), and the resulting HOMO–LUMO gaps showed only a slight reduction (0.17–0.04 eV) for the —COOH functionalized GQDs compared to the bare systems.

In a typical $^1O_2$ generation process, excitons from singlet branch (S_n) convert into triplet states (T_n) via intersystem crossing (ISC) for a fluorophore, which then transfers its energy to surrounding oxygen species in their triplet ground state[48] (Figure 2a). For a heavy-metal-free $^1O_2$ synthesizer such as GQDs, the rate of this process is mainly controlled by the spin–orbit coupling (SOC) between the singlet and triplet excited states of the synthesizer as indicated by Fermi's golden rule[48–50] (Equation 1)

$$k_{ISC} = \frac{2\pi}{\hbar}\left|\left\langle T_n|\widehat{H_{soc}}|S_m\right\rangle\right|^2 \rho_{FC} \quad (1)$$

where $\langle T_n|\widehat{H_{soc}}|S_m\rangle$ is the SOC matrix element between a given singlet and triplet excited state, and ρ_FC is the corresponding Franck-Condon weighted density of states. In that regard, we calculated the SOC matrix elements (V_{SOC}) for model GQD systems using perturbative zeroth-order regular approximation (ZORA) Hamiltonian. In the case of non-functionalized GQDs, calculated V_{SOC} between T_1 and S_1 states are 0.03, 0.03, and 0.05 cm^{-1} for C54, C96, and C120, respectively (Figure 2f). Additionally, V_{SOC} values for other states are also negligible for non-functionalized GQDs (Table S4, Supporting Information). Interestingly, the calculated V_{SOC} exhibited a drastic increase with —COOH functionalization (Figure 2f) and this increase was 20–30 fold for cGQDs with 12 —COOH units compared to the systems with no functionalization, which supports the experimentally concluded $^1O_2$-QY of the cGQDs in comparison with non-functionalized GQDs. Meanwhile, the energy difference between T_1 and S_1 states (ΔE_{ST}) remained mainly unaltered with —COOH functionalization (Figure S8b,d,f, Supporting Information). We note that V_{SOC} between other states also exhibited an increasing trend with —COOH functionalization as indicated by the average V_{SOC} between the lowest five singlet and triplet states (Figure S9, Supporting Information). These calculations confirm high singlet oxygen production by cGQDs, attributed to the significant increase in spin–orbit coupling when GQDs are functionalized with -COOH groups.

2.6. Cytotoxicity and Bactericidal Activity Assessment of cGQD Suspension

Examining the cytotoxicity of cGQDs is important to determine their suitability for biological applications. For this purpose, we investigated different cGQD concentrations on mouse embryonic fibroblast cells (3T3-J2) using the CellTiter-Glo 2.0 assay (Figure S10, Supporting Information), which is a luminescent assay to measure cell viability by quantifying ATP and indicates metabolically active cells. Colloidal cGQDs with concentrations of up to 60 μg mL^{-1} maintained cell viability of over 80% in both dark and light conditions (**Figure 3a**). To assess long-term cytotoxicity, cell viability tests conducted at 48 and 72 h indicated sustained high viability, suggesting minimal cytotoxic effects over extended periods (Figure S11, Supporting Information). Moreover, confocal microscopy showed internalization of cGQDs by cells into the cytoplasm and no accumulation on cell membrane (Figure S12, Supporting Information). We further investigated the effect of different illumination times at a predetermined safe concentration of 25 μg mL^{-1}. A slight decrease, with 90% cell viability, was observed of cells incubated with cGQDs for 30 min compared to the cells in dark (Figure 3b). In addition, LDH enzyme release, which is indicative of membrane disruption, was measured after under blue light illumination at different time points. We observed a significant increase in LDH release in a time dependent manner in the presence and absence of cGQD treated groups, which showed the cellular stress directly after light exposure (Figure 3c). However, this condition did not affect cell viability after 24 h incubation (Figure 3d). Even after 72 h, we observed cell viability over 60% for the samples treated with cGQDs and light.

After assessing the safe concentration levels on mammalian cells, a minimal bactericidal concentration (MBC) assay was performed with bacterial strains *S. aureus* and *E. coli*, species representative of Gram-positive and Gram-negative, respectively (Figure 3e). Bacteria were added to 10-fold serial dilutions of colloidal cGQD, the mixture was illuminated for 30 min and plated on blood agar. After 30 min of illumination, 99.9% of the *S. aureus* inoculum was killed at 0.4 μg mL^{-1} and the entire *S. aureus* inoculum was eradicated at 0.8 μg mL^{-1} (Figure 3f). To the best of our knowledge, 0.4 μg mL^{-1} is the lowest MBC reported against *S. aureus* using quantum dots (Table S5, Supporting Information). *E. coli* was relatively less susceptible to cGQDs and a 4-log reduction (≈ 99.998% killing) of CFU was observed at 25 μg mL^{-1} (Figure 3f). cGQDs were then tested using the predetermined MBC and most potent cGQD concentrations (0.8 μg mL^{-1} for *S. aureus* and 25 μg mL^{-1} for *E. coli*) in an illumination time-dependent assay. cGQDs exhibited stronger antimicrobial activity against both *S. aureus* and *E. coli* with increasing illumination time, ultimately achieving at least 4-log reduction in the inocula (Figure 3g). Hence, cGQDs can eradicate the bacteria at safe concentrations and light illumination levels.

2.7. Cytotoxicity and Bactericidal Activity of cGQD Film

Medical devices such as biomaterial implants, wound dressings, catheters, urinary stents, and dental implants are commonly used in various clinical applications and have an increased risk of bacterial infection.[51–54] To prevent and/or treat bacterial colonization on medical implant surfaces we developed cGQDs assembled antimicrobial films. For the production, cGQDs were coated on top of a TiO_2 base layer via a layer-by-layer approach. Polydiallyldimethylammonium chloride (PDDA), a non-toxic polycation polymer molecule, demonstrates great compatibility with negatively charged cGQDs via electrostatic interaction. The layer-by-layer assembly was accomplished by using an automatic dip coater machine, which is a quick, simple, and cost-effective method for fabricating multilayer coated films on a wide range of surfaces (**Figure 4a**). Five layers of cGQDs and four alternating layers of PDDA (Figure 4b), revealed a consistently increasing optical absorbance due to increased thickness (Figure S13, Supporting Information). The photographs of the cGQD films

© 2025 The Author(s). Advanced Functional Materials published by Wiley-VCH GmbH

16163028, 2025, 26, Downloaded from https://advanced.onlinelibrary.wiley.com/doi/10.1002/adfm.202421537 by Koc University, Wiley Online Library on [02/09/2025]. See the Terms and Conditions (https://onlinelibrary.wiley.com/terms-and-conditions) on Wiley Online Library for rules of use; OA articles are governed by the applicable Creative Commons License

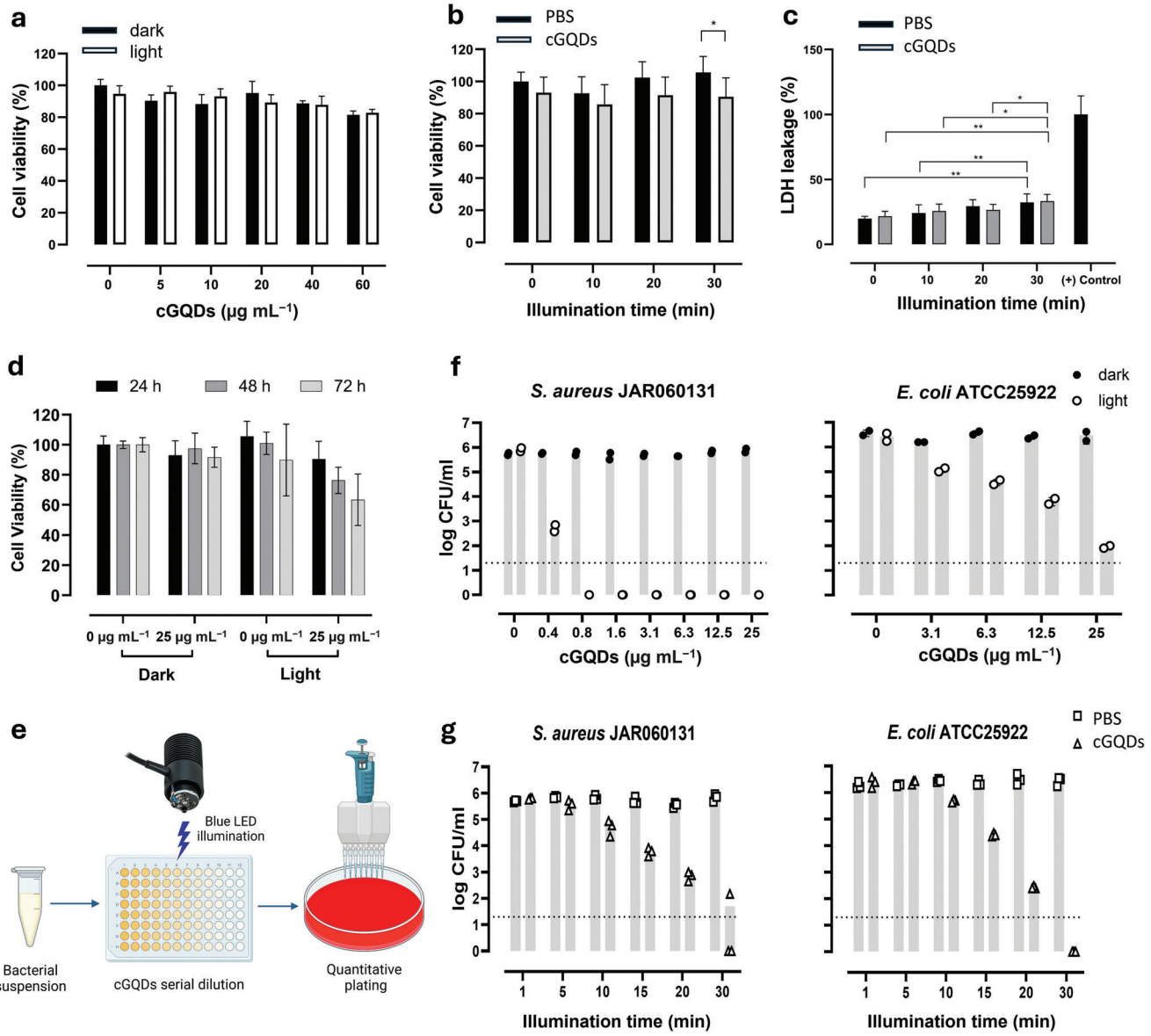

Figure 3. Cytotoxicity and antimicrobial activity of cGQD solution. a) Cell viability results of 3T3-J2 cells treated with different concentrations of cGQD (5, 10, 20, 40, and 60 μg mL^{-1}) with and without blue light illumination for 10 min. b) Cell viability of cells treated with 25 μg mL^{-1} of cGQDs or 0 μg mL^{-1} (PBS) as negative control with different illumination times. c) LDH leakage of cells treated with 25 μg mL^{-1} of cGQDs or 0 μg mL^{-1} (PBS) with different illumination times. Lysed cells were used as positive (+) control set at 100% to compare LDH leakage percentage due to cGQDs at different time points. d) Viability of cells over time after treatment with 25 or 0 μg mL^{-1} (PBS) of cGQDs as negative control with and without blue light illumination for 30 min. e) Schematic illustration of antibacterial experiments for minimum bactericidal concentration (MBC) assay on cGQD solution. f) Bactericidal activity of cGQDs against *S. aureus* and *E. coli* with and without blue light illumination for 30 min. Survival of bacteria is shown in log CFU. Bars represent mean values of one experiment with duplicate measurements. g) Time-series antibacterial experiments on *S. aureus* treated with 0.8 μg mL^{-1} of cGQDs and *E. coli* treated with 25 μg mL^{-1} of cGQDs. PBS was used as a negative control without cGQDs. Statistical analysis using ordinary one-way ANOVA test showed significant difference between indicated conditions, $*p \leq 0.05$, $**p \leq 0.01$. Survival of bacteria is shown in log CFU. Bars represent mean values of one experiment performed in triplicate. Dashed line represents the detection limit of <20 CFU. A value of 1 was assigned when no colonies were found (below detection limit).

revealed homogeneous coatings over large surface areas (inset of Figure 4c). We also tested the physical stability of the cGQD films (Figure S14, Supporting Information), and they exhibited remarkable stability even when subjected to sonication in a water bath. cGQD film with 5 layers was compared with a 1-layer for singlet oxygen generation by using ABDA probe, and 5-layer film produces higher singlet oxygen upon blue light illumination due to stronger absorption with a thicker photoactive layer (Figure 4c). A CTG viability assay with 3T3-J2 cells with cGQD coated films (either 5 layers or 1 layer) was assessed both with and without illumination for 10 min. In comparison to 1 layer, 5-layer film exhibited higher cell viability (Figure 4d). In terms

© 2025 The Author(s). Advanced Functional Materials published by Wiley-VCH GmbH

16163028, 2025, 26, Downloaded from https://advanced.onlinelibrary.wiley.com/doi/10.1002/adfm.202421537 by Koc University, Wiley Online Library on [02/09/2025]. See the Terms and Conditions (https://onlinelibrary.wiley.com/terms-and-conditions) on Wiley Online Library for rules of use; OA articles are governed by the applicable Creative Commons License

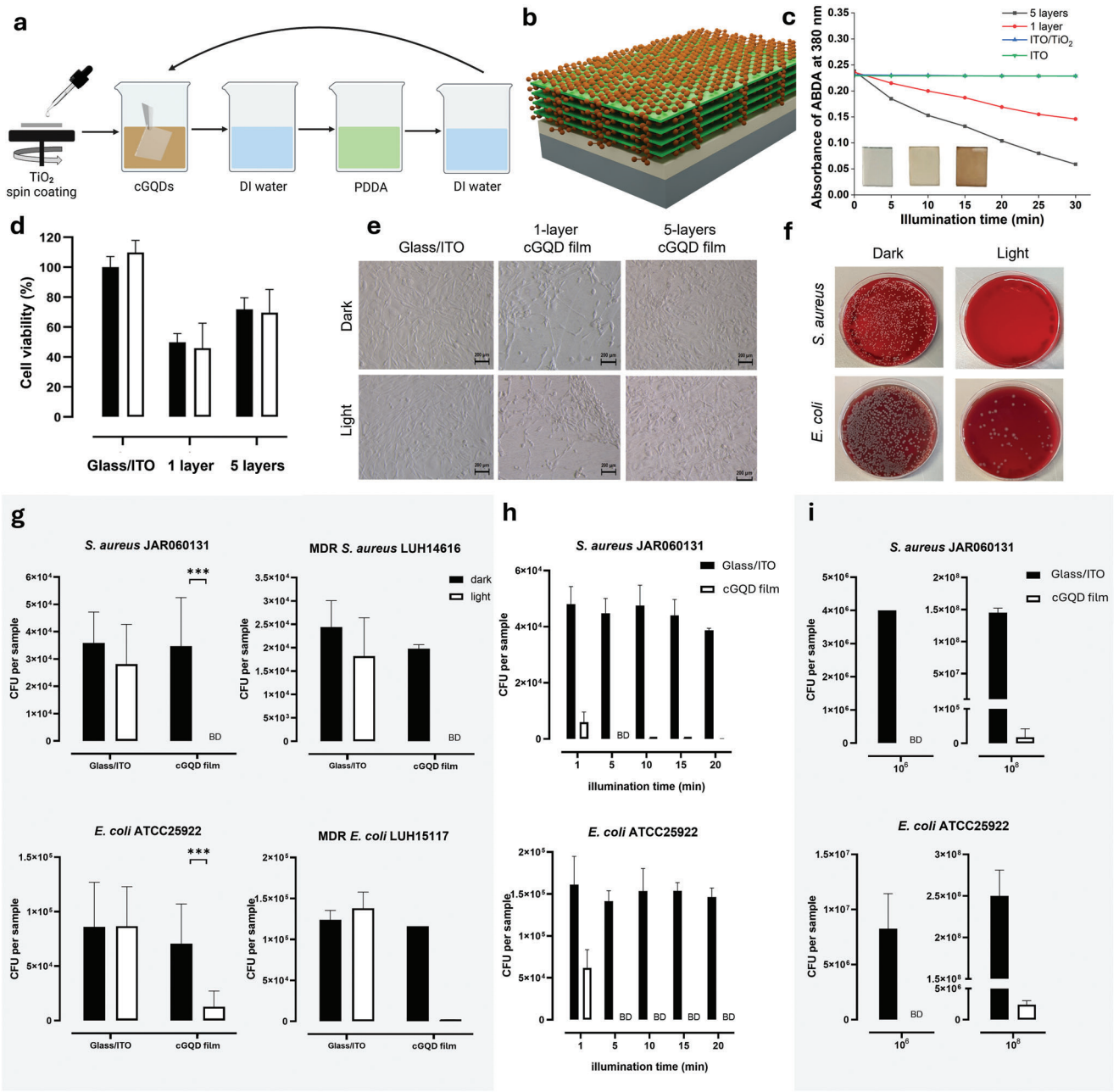

Figure 4. cGQDs film fabrication, viability of exposed mammalian cells, and antibacterial activity. a) Spin coating of TiO_2 on ITO substrate followed by dip coating of cGQDs and PDDA. b) Schematic of layer-by-layer coated cGQD film. c) Absorbance of ABDA singlet oxygen probe at 380 nm over time by films of cGQDs composed of 5 layers and 1 layer. ITO and ITO/TiO_2 served as negative control surfaces. Inset shows the photographs of Glass/ITO slide, 1-layer cGQD film, and 5-layer cGQD film (from left to right). d) Relative cell viability of 3T3-J2 cells upon exposure to 1-layer and 5-layer films with or without blue light illumination for 10 min analyzed with CTG cytotoxicity assay. Glass/ITO served as negative control. e) Bright field images of treated 3T3-J2 cells with cGQD films (1-layer and 5-layers) under blue light and dark conditions. Scale bar = 200 µm. f) Blood agar images of *S. aureus* and *E. coli* CFU after treatment with cGQD film (5-layers) under 30 min blue light and dark conditions. g) Bactericidal activity of cGQD films (5-layers) against S. aureus and E. coli with or without illumination for 30 min. Inocula ranged from 3.1×10^4 to 4.8×10^4 CFU for experiments with *S. aureus* and from 8.8×10^4 to 2×10^5 CFU for experiments with *E. coli*. Statistical analysis using the Mann-Whitney test showed significant difference between indicated conditions. Data of 3 or 4 independent experiments with antibiotic susceptible strains performed in duplicate. $***p \leq 0.001$. Data of one independent experiment with MDR strains S. aureus LUH14616 and *E. coli* LUH 15117, with duplicate measurements. h) The effect of illumination time on bactericidal activity for S. aureus and E. coli. The cGQD films (5-layers) were inoculated with 10^4 CFU and exposed to light or dark for different time periods. Inoculum was 6.25×10^4 CFU for S. aureus and 1.6×10^5 CFU for *E. coli*. i) The killing capacity of the cGQD films against high numbers of *S. aureus* and *E. coli*. The materials were inoculated with either 10^6 CFU or 10^8 CFU and illuminated for 30 min. Inoculum was 2.8×10^6 or 1.5×10^8 CFU for *S. aureus* and 7.5×10^6 or 2.7×10^8 CFU for *E. coli*. Data of one independent experiment with duplicate measurements. Bars represent median value. Error bars represent standard deviation. Bactericidal assays had a detection limit of <20 CFU. BD; below detection limit, MDR; multidrug resistant.

© 2025 The Author(s). Advanced Functional Materials published by Wiley-VCH GmbH

16163028, 2025, 26, Downloaded from https://advanced.onlinelibrary.wiley.com/doi/10.1002/adfm.202421537 by Koc University, Wiley Online Library on [02/09/2025]. See the Terms and Conditions (https://onlinelibrary.wiley.com/terms-and-conditions) on Wiley Online Library for rules of use; OA articles are governed by the applicable Creative Commons License

of cell morphology, although the cells exhibited a fibroblast-like appearance on the ITO control, a notable decline in cell adhesion was observed, resulting in round-shaped cells under both dark and light conditions (Figure 4e).

To assess bactericidal activity of the cGQD films, we performed the JIS Z 2801:2000 surface microbicidal activity assay. The 5-layer cGQD film killed the entire *S. aureus* inoculum after 30 min of illumination (Figure 4f,g). Like in case of the suspension, *E. coli* appeared less sensitive than *S. aureus* to the films (Figure 4f,g). For both species, the antibiotic susceptible strain and the MDR strain were killed by the 5-layer cGQD film with the same efficiency. The control group (glass coated with ITO) showed no significant killing of *S. aureus* or *E. coli* bacteria (Figure 4g). We assessed the minimal illumination time necessary to achieve at least a 99.9% reduction of bacterial numbers from a 10^4 inoculum. The film was tested in the JIS surface microbicidal assay with 1, 5, 10, 15 and 20 min of illumination. Five min of illumination was sufficient to achieve at least 99.9% reduction for both *S. aureus* and *E. coli* (Figure 4h). To assess the bactericidal capacity of the film, we tested inocula of 10^6 and 10^8 CFU of *S. aureus* and of *E. coli*. The cGQD film killed the 10^6 CFU inoculum of *S. aureus* until below the detection limit and reduced the 10^8 CFU *S. aureus* inoculum to less than 10^5 CFU in 30 min (Figure 4i). For *E. coli*, the 10^6 inoculum was reduced to below the detection limit and the 10^8 inoculum was reduced to 10^6 CFU (Figure 4i). Apparently, the inoculum of 10^8 CFU is just the edge surpassing the capacity of the coating, where 99% of the highly concentrated inoculum eradicated.

The approach of fabricating light-activatable cGQD film on biomedical devices such as transcutaneous devices like catheters or orthopedic medical devices holds great potential to prevent/treat bacterial infections by an efficient, non-invasive, biocompatible and cost-effective method. Colloidal cGQD may be incorporated in creams, gels or wound dressings to allow skin applications. The observed strong reduction of even very high inocula (10^8 CFU) in the antibacterial experiments are promising for wound dressing applications as most wounds that develop infections have tissue colonization of less than 10^5 CFU per gram of tissue.[55] Medical devices placed transcutaneously will likely be in contact with lower numbers of bacteria[56] and for those devices the light to the cGQD surfaces can be delivered via optical fibers and waveguides.[57] Moreover, the numbers of skin bacteria contaminating medical devices are generally lower. Therefore, the cGQD film has great potential for preventing infection in such clinical applications. Our results thus warrant preclinical studies on anti-infective efficacy in animal models, including analysis of potential in vivo toxicity and pharmacokinetics of the cGQD.

3. Conclusion

In this study, photoactive antimicrobial carboxyl-functionalized GQDs were synthesized via a hydrothermal reaction using trinitropyrene in an $NaHCO_3$ aqueous solution. The synthesis led to the cGQDs with an exceptionally high singlet oxygen quantum yield of 0.88, which is 20-fold higher than the non-functionalized GQDs. Our time-dependent density functional theory calculations indicated that the elevated singlet oxygen quantum yield originates from enhanced spin–orbit coupling between singlet and triplet states compared to the systems with no functionalization. These cGQDs provided cell viability over 80% at concentrations up to 60 μg mL^{-1} in both dark and light conditions. Due to the high singlet oxygen generation efficiency, the entire inoculum of *S. aureus* was successfully eradicated using cGQDs suspension with a concentration as low as 0.8 μg mL^{-1} upon light illumination. Remarkably, the minimum bactericidal concentration (MBC) of cGQDs (0.4 μg mL^{-1}) against *Staphylococcus aureus* is the lowest MBC reported to date using light activated quantum dots. The cGQDs were transferred to nano-assembled coatings via layer-by-layer deposition and the cGQD thin films also maintained their biocompatibility. The 5-layer cGQD thin films killed over a 99.9% of both susceptible and multi-drug resistant *S. aureus* and *E. coli* inocula under low-intensity light illumination of 5 mW cm^{-2}. From a practical point of view, potent bactericidal activity of cGQD films combined with their coating potential on a wide variety of medical devices show high promise to suppress the frequent bacterial infections in biomedical devices (e.g., urinary catheter). In addition, the antibacterial activity of the cGQDs in suspension can also allow application to skin infections and burns. Overall, the exceptional singlet oxygen generation and strong bactericidal activity of these cGQDs, both in suspension and as coatings, highlight their strong potential for future antibacterial applications.

4. Experimental Section

cGQDs Synthesis: The carbon source, pyrene (2g, Sigma Aldrich) was converted into 1,3,6 trinitropyrene, as previously demonstrated by Wang et al.[21] in hot HNO_3 (160 mL) at 90 °C under stirring and refluxing overnight. After cooling it down to room temperature, to remove the acidic contents, the solution was diluted with 1 L of DI water filtered through a 0.22 μm filter paper using vacuum suction. Then, the residue on top of filter paper was dried for 3 days in vacuum chamber to get powder form of 1,3,6-trinitropyrene. To get carboxyl group functionalization on edges of GQDs, we used aqueous $NaHCO_3$ as a solvent during hydrothermal synthesis. Briefly, 267 mg of dried 1,3,6 trinitropyrene was dispersed in $NaHCO_3$ solution (0.08 M, 50 mL), followed by ultrasonication bath for 1 h until the solute homogeneously dispersed in the solvent. The suspension was then transferred to 80 mL poly(tetrafluoroethylene) (Teflon)-lined autoclave, put into furnace (Protherm, ECO series), and heated at 200 °C for 10 h. Autoclave was naturally cooled down within the furnace. After cooling down to room temperature, the obtained solution was filtered through a 0.22 μm filter paper to remove large particles and other residual elements. To remove the sodium salts and unfused small molecules, the filtrate was further subjected to dialysis bag of 3.5K MWCO (SnakeSkin Dialysis Tubing) for 3 d. The final solution was stored for further use and characterizations.

Structural and Photophysical Characterization: TEM and HRTEM measurements were performed using a HITACHI HF5000 200 kV (S)TEM. For atomic force microscopy (AFM) analysis, cGQDs were spray coated on clean silicon wafer and measured using a Bruker Dimension Icon AFM. The Fourier transform infrared (FT-IR) spectrometer was performed with a lyophilized (and vacuum dried overnight) cGQDs powder using a FTIR-ATR and Microscope. Raman spectroscopy was measured using Renishaw Invia-Raman microscope after coating cGQDs on a clean silicon wafer using with an excitation laser wavelength of 633 nm. For the X-ray photoelectron spectroscopy (XPS) measurement, cGQDs were coated on silicon wafer and dried fully in vacuum oven overnight. XPS measurements were performed using a Thermo Scientific K-α (Al Kα source) surface analysis tool at ultrahigh vacuum conditions. Steady-state absorbance and PL measurements were performed using an Edinburgh Instruments, FS5 spectrofluorometer with a 150 W xenon lamp. The excitation wavelength was 450 nm. For absorbance and PL measurements, regular quartz cuvettes were used. PLQY measurements were carried out using an integrating

© 2025 The Author(s). Advanced Functional Materials published by Wiley-VCH GmbH

16163028, 2025, 26, Downloaded from https://advanced.onlinelibrary.wiley.com/doi/10.1002/adfm.202421537 by Koc University, Wiley Online Library on [02/09/2025]. See the Terms and Conditions (https://onlinelibrary.wiley.com/terms-and-conditions) on Wiley Online Library for rules of use; OA articles are governed by the applicable Creative Commons License

sphere with an inner diameter of 150 mm. Time-dependent photoluminescence (PL) decay reading was taken using a PicoQuant MicroTime 100 time-resolved confocal fluorescence microscope.

Singlet Oxygen Measurement: For singlet oxygen detection and quantification, 9,10-anthracenediyl-bis(methylene)dimalonic acid (Sigma Aldrich 75068) was used as a sensor probe. Blue (450 nm) and green (530 nm) LED light sources (Thorlabs) were controlled by an LED driver (Thorlabs LED Driver for high-power and mounted LEDs). Intensity of light sources to illuminate cGQDs, non-functionalized GQDs, and rose bengal (RB) were adjusted to achieve equal number of absorbed photons (Table S1, Supporting Information). Absorption spectra were recorded using a Synergy H1 Microplate Reader (BioTek). ABDA (25 µM) was added to cGQDs (25 µg mL^{-1}), non-functionalized GQDs (25 µg mL^{-1}), and RB (25 µM; 24.3 µg mL^{-1}) in a 96 well plate (black-walled, clear-bottom 96-well microplates). All values represent final concentrations. Absorbance of the samples were determined at the photoexcitation wavelengths (450 nm for cGQDs and non-functionalized GQDs, and 530 nm for RB). Absorbance profiles of the solutions (350–525 nm) were recorded in dark and then illuminated with blue light (5 mW cm^{-2}) for cGQDs and non-functionalized GQDs, and with green light (5.14 mW cm^{-2}) for RB. The absorbance of the ABDA probe was recorded for 30 min at 5 min intervals to observe photodegradation trend. Singlet oxygen quantum yield of GQDs was calculated using the following formula, with rose bengal as the standard photosensitizer.

$$\Phi\,(\mathrm{GQDs}) = \Phi\,(\mathrm{RB})\,\frac{\mathrm{A\,(RB)} * \mathrm{K\,(GQDs)}}{\mathrm{A\,(GQDs)} * \mathrm{K\,(RB)}} \quad (2)$$

whereas Φ(RB) is the known singlet oxygen quantum yield of rose bengal (0.75 in water). A(GQDs) and A(RB) are the absorbance of GQDs and RB at the photoexcitation wavelengths, respectively. While K(GQDs) and K(RB) are the decomposition rate constant of ABDA probe due to GQDs and rose bengal, respectively.

DFT/TDDFT Computational Methods: All computations were performed using ADF 2023 software with B3LYP functional and DZP basis set. The initial geometries for non-functionalized model GQDs (C54, C96, and C150) exhibit D_{6h} point group symmetry, and the geometries were optimized using this symmetry constraint. In comparison, the geometry optimizations for each —COOH functionalized GQD were carried out without any symmetry constraints. Excited-state calculations were performed with time-dependent density functional theory (TDDFT) as implemented in ADF software using optimized ground-state geometries. The spin–orbit coupling matrix elements (V_{soc}) between singlet and triplet states were calculated by employing the perturbative Hamiltonian of zeroth-order regular approximation (ZORA).

Bacteria: *S. aureus* JAR060131 (number 890; Culture Collection of Switzerland [CCOS], Wädenswill, Switzerland, susceptible to all tested antibiotics except benzylpenicillin), MDR *S. aureus* LUH14616 (resistant to benzylpenicillin, oxacillin, gentamicin, tobramycin, ciprofloxacin, levofloxacin, tetracyclin and rifampicin), *E. coli* ATCC25922 (susceptible to all tested antibiotics) and MDR *E. coli* LUH15117 (resistant to ampicillin, amoxicillin, piperacillin, cefuroxime, cefotoxitin, cefotaxime, ceftazidime, gentamicin, tobramycin, ciprofloxacin, colistin and trimethoprim) were used in this study. Bacteria were stored in nutrient broth with 20% (v/v) glycerol at -80 °C. Before each experiment, bacteria were grown to the mid-logarithmic growth phase in tryptic soy broth (TSB, BD Difco) at 37 °C while shaking at 120 rpm.

Minimal Bactericidal Concentration (MBC) Assay: Bacteria cultured to the mid-logarithmic growth phase were diluted with TSB to 1 × 10^7 CFU mL^{-1}, based on the optical density of the suspension at 620 nm (OD_{620nm}). The exact concentration of the bacteria added to the experiment (inoculum) was assessed by quantitative plating of quadruplicate 10 µL droplets of 10-fold serial dilutions on blood agar plates, incubating overnight at 37 °C and counting CFU the following day. Colloidal cGQDs were suspended in deionized water. Ten microliter of the bacterial suspension (final concentration of approximately 1 × 10^6 CFU mL^{-1}) was added to 90 µL of colloidal cGQDs (final concentration range of 0.4–200 µg mL^{-1} diluted in PBS) in a polystyrene 48-wells flat bottom plate (VWR). As growth control, bacteria were added to PBS without cGQDs. The plate was kept in the dark for 30 min or illuminated from above at 3 cm distance from the sample with 435 nm blue light (LumiSource, PCI Biotech, 5 mW cm^{-2}) under stationary conditions. After incubation, 10 µL samples were taken from each well and plated undiluted or 10-fold serially diluted on blood agar plates. The blood agar plates were incubated overnight at 37 °C and inspected for bacterial growth the following day. The MBC_{GQDs} is defined as the lethal concentration of the suspension that kills 99.9% (3-log) of the bacterial inoculum. All mentions of log refer to log10 values. The detection limit was 20 CFU. A value of 1 was assigned when no colonies were found.

cGQD Films Fabrication: Commercially available ITO substrates were cleaned with detergent solution, DI water, acetone, and ethanol, respectively for 15 min each, followed by UV generated ozone cleaning to eliminate organic impurities from the surface and to improve its work function. Then cleaned ITO was coated with 40 µL of TiO_2 (100 mg titania in 1 mL of ethanol) using spin coater with 2000 rpm for 30 s and baked at 60 °C for 1 min, 100 °C for 5 min, 200 °C for 5 min, and finally at 450 °C for 30 min. PDDA solution was prepared separately by mixing 2% PDDA (Sigma Aldrich 409014, 20 wt% in H_2O, *M*w = 10 0000) in 0.5 M solution of NaCl followed by ultrasonication bath for 30 min. Automatic dip coater machine enabled with programable features was used for coating of multiple layers of as-prepared cGQDs and PDDA solution on top of the ITO/TiO_2 surface. More precisely, ITO/TiO_2 was dipped into cGQDs (400 µg mL^{-1}) and PDDA solution for 10 min each, followed by rinsing in DI water for 3 min after both steps. The same deposition cycle was repeated 4 times to achieve five layers of cGQDs and four separation layers of PDDA in between the cGQDs consecutive layers. Finally, the samples were dried with nitrogen gas and kept in vacuum desiccator for further use.

cGQD Films Bactericidal Activity Assay: The Japanese Industrial Standard assay (JIS Z 2801:2000 (Japanese Standards Association 2000)) was used with modifications to assess surface bactericidal activity of cGQDs coated glass materials. In short, bacteria in the mid-logarithmic growth phase were diluted with PBS to 1 × 10^6 CFU based on the $OD_{620\,nm}$. The exact bacterial inoculum added to the experiment was assessed as described above by quantitative culture. Each material was placed in a six-wells plate and 50 µL of the bacterial suspension, containing 5 × 10^4 CFU, was spread on the material, covering at least 90% of the surface (3 cm^2). The number of bacteria added to the material was calculated based on 1.5 × 10^4 CFU cm^{-2}, as described by JIS Z 2801:2000. In contrast to the JIS standard, we did not cover the sample with parafilm to prevent blocking of the blue light. Glass coated with ITO served as the control. After 30 min of illumination from above at 3 cm distance from the cGQDs film surface with 435 nm blue light (LumiSource, PCI Biotech, 5 mW cm^{-2}) or after incubation in the dark, 2 mL PBS was added to each sample, and these were sonicated for 5 min at 35 kHz in a sonicator water bath (Elma, Transsonic 460) to dislodge adherent bacteria. 2 mL of sonicate fluid was collected in Eppendorf tubes, vortexed and 100 µL was plated undiluted and 10-fold diluted on blood agar plates. The blood agar plates were incubated overnight at 37 °C and the numbers of CFU were counted the next day using ImageJ (v1.53t). Images were converted to 16-bit gray scale and then to a binary image. Colonies too close together were separated using the watershed tool. Particles were analyzed digitally to obtain the colony count. The limit of detection was 20 CFU. In addition, to assess whether any viable bacteria had remained on the glass materials after sonication, the material was incubated overnight in 5 mL TSB at 37 °C, shaking at 120 rpm. Visual bacterial growth was evaluated the next day. Figures 4g,h,i show "BD" (below detection limit) when no colonies were found.

Culture of 3T3-J2 Cells: Mouse embryonic fibroblast cells (3T3-J2) were cultured in Dulbecco's modified Eagle's medium (4.5 g L^{-1} D-Glucose) supplemented with 10% (v/v) bovine calf serum, penicillin (100 IU mL^{-1}) and streptomycin (100 µg mL^{-1}) at 37 °C in a 5% CO_2 incubator until 80–90% confluency.

Colloidal cGQDs Cell Viability Assessment: Cells were seeded on an opaque 96 well plate (5000 cells per well) and incubated at 37 °C in a 5% CO_2 incubator overnight. After incubation, they were treated with different concentrations of cGQDs solutions (5, 10, 20, 40, and 60 µg mL^{-1}) prepared in a complete medium Dulbecco's modified Eagle's medium

© 2025 The Author(s). Advanced Functional Materials published by Wiley-VCH GmbH

16163028, 2025, 26, Downloaded from https://advanced.onlinelibrary.wiley.com/doi/10.1002/adfm.202421537 by Koc University, Wiley Online Library on [02/09/2025]. See the Terms and Conditions (https://onlinelibrary.wiley.com/terms-and-conditions) on Wiley Online Library for rules of use; OA articles are governed by the applicable Creative Commons License

(high glucose) supplemented with 10% (v/v) bovine calf serum, penicillin (100 IU mL^{-1}) and streptomycin (100 µg mL^{-1}) for 24 h at 37 °C, 5% CO_2. After treatment, light-illuminated group were exposed to 450 nm visible light (5 mW cm^{-2}) for 10 min. Cells were further cultured for 24, 48, and 72 h, and the viability was analyzed with CellTiter-Glo (CTG) Luminescent Cell Viability Assay (Promega, Mannheim, Germany) according to manufacturer's instructions. For the experiment, cells were taken from the incubator and left at room temperature for 30 min. Then, CellTiter-Glo Reagent was added to each well and the plate was put on the orbital shaker for 5 min and incubated in RT for 10 min for stabilization of luminescence signals. Synergy H1 Microplate Reader (Bio-Tek Instruments) was used to measure the luminescence signals. The relative cell viability was calculated by comparing the luminescence signals (RLUs)'s of experimental groups with the untreated control group.

To check single dose with different illumination durations cells were seeded on an opaque 96-well plate (5000 cells per well) and incubated overnight at 37 °C in a 5% CO_2 incubator. After incubation, they were treated with 200 µL 25 µg mL^{-1} concentration of cGQDs prepared in a fresh culture medium. Cells were directly exposed to 450 nm blue light at 5 mW cm^{-2} for 10, 20 and 30 min. After illumination 100 µL of cell solution was collected for LDH cytotoxicity assay. Then cells were incubated further in treatment condition for 24 h, 48 h and 72 h at 37 °C, 5% CO_2 to examine cell viability with CTG assay. The control group was cells grown in only a culture medium without cGQDs. The dark condition has the same treatment steps without blue light illumination.

Lactate-Dehydrogenase Release Assay: For Lactate-dehydrogenase Release Assay, CytoSelect LDH Cytotoxicity Assay Kit (CBA-241, Cell Biolabs) was used to examine the cell membrane stability of cells after GQD and light treatment. After the end of light illumination in the time series, 100 µL of culture medium was taken from each sample and immediately put on ice to eliminate enzymatic degradation until the end of all experiments (<130 min). 90 µL of culture medium was taken from each sample and added to transparent 96-well cell culture plates. Thereafter, 4 µL of LDH cytotoxicity assay reagent was added to each well, and the plates were incubated at 37 °C in a 5% CO_2 incubator for 30 min to allow the reaction to occur. As a positive control of the experiment, cells were incubated with a culture medium containing 1% Triton-X-100 to induce LDH leakage for 10 min at 37 °C in a 5% CO_2. Negative control was culture media collected from untreated cells. The Synergy H1 Microplate Reader (BioTek) device was used to measure LDH leakage into the culture medium at 450 nm optical density. Relative cytotoxicity (%) was calculated by the following equation:

$$\text{Relative cytotoxicity (\%)} = \frac{\text{OD experimental sample} - \text{OD negative control}}{\text{OD positive control} - \text{OD negative control}} \times 100 \quad (3)$$

Cell Uptake and Confocal Microscopy Imaging: To show cGQDs uptake by cells, 3T3-J2 cells were seeded on 12 mm cover glasses in 24 well plate (10 000 cells per well) and treated with 25 µg mL^{-1} cGQDs in a complete medium for 30 min at 37 °C, 5% CO_2. After incubation, the remaining QDs were removed by twice PBS washing. Then a live cell imaging solution (Gibco, USA) was added, and cells were observed under a confocal laser scanning microscope (Leica DMI8 SP8) using lasers of 488 nm and 594 nm. Internalization of QDs were observed with Z-stack in different parts of cytosol.

GQD Films Cell Viability Assessment: The substrates were sterilized first by cleaning with ddH2O, 70% ethanol followed by air-drying. The surface was further sterilized under UV illumination for 30 min. Substrates, equal size of 20 mm x 15 mm, were placed in wells of the six-well plates and nail polished on one side to prevent rotation within the wells during the experiments. 3T3-J2 cells were seeded as 200 000 cells per well on poly-L-lysine (PLL, Sigma-Aldrich, MO, USA) coated samples. After 24 h of incubation, cells on substrates were illuminated from the bottom as 450 nm blue light, 5 mW cm^{-2} for 10 min using Thorlabs M450LP1 LED. Cells were further cultured for 24 h, and viability was analyzed with CTG assay.

Statistics: The statistical analysis for bacterial experiments was performed in Graphad Prism v9.3.1 using the Mann-Whitney test with False Discovery Rate (FDR) approach. Differences were considered statistically significant at $p \leq 0.05$. Statistical analysis for cell culture data was performed in GraphPad Prism 9.5.1 using ordinary one-way ANOVA with Tukey's post-hoc multiple comparison. All treatment concentrations were compared to 0 µg mL^{-1} and $p < 0.05$ was considered statistically significant. *$p < 0.05$, **$p < 0.01$, ***$p < 0.001$, ****$p < 0.0001$.

Supporting Information

Supporting Information is available from the Wiley Online Library or from the author.

Acknowledgements

This project has received funding from the European Union's Horizon 2020 research and innovation program under the Marie Skłodowska-Curie grant agreement No. 955664 (STIMULUS). This publication is also a part of the project DARTBAC (with project number NWA.1292.19.354) of the research program NWA-ORC which is (partly) financed by the Dutch Research Council (NWO). The authors thank Gülcan Çorapcıoğlu for the TEM analysis and Dr. Hande Gündüz for the FTIR-ATR measurement (both from Koç University Nanofabrication and Nanocharacterization Center for Scientific and Technological Advanced Research). The authors also thank Dr. Barış Yağcı for the XPS measurements and Dr. Hamaneh Zarenezhad for the AFM readings (both from KUYTAM, Koç University Surface Science and Technology Center). The authors thank Ugur Berkay Caliskan from IDEALAB Koç University for cGQD film image design. The authors also thank Peter H. Nibbering from the Department of Infectious Diseases, Leiden University Medical Center, Leiden, The Netherlands, for the *S. aureus* LUH 14616 and *E. coli* LUH 15117 bacterial strains. The authors also thank Prof. Dr. Ibrahim Halil Kavakli for providing access to the Synergy microplate reader for ROS analysis.

Conflict of Interest

The authors declare no conflict of interest.

Author Contributions

S.N. and S.A.J.Z. designed the project, wrote and reviewed the orignial draft, and supervised M.H. and L.S.v.H for experiments, analysis, and interpretation. M.H. and L.S.v.H. contributed equally to design and perform experiments, data collections, and analysis, and jointly wrote first draft of the manuscript. M.H., Z.E., and T.K. performed the synthesis and structural characterization of cGQDs and intrepreted the data. M.H. conducted photophysical and photochemical analysis of cGQD suspension and film. M.H. fabricated cGQD films, analyzed and interpreted data. O.M. wrote, reviewed, revised the orginal draft and the revised manuscript, supervised M.H., Z.E., and T.K. for the synthesis and structural characterization of cGQDs, and interpretation of the data. L.S.v.H. conducted antibacterial experiments on cGQD suspensions and films, analyzed and interpreted the data. H.N.K. performed cell viability experiments and analyzed the data. F.A. performed density functional theory simulations. All authors contributed to analysis and interpretation of data, contributed to writing part of specific sections in the manuscript. Additionally, all authors discussed the results, reviewed and edited manuscript at various stages of the project.

Data Availability Statement

All data related to the materials and methodologyof this work are mentioned in the main text. More data that support the results of this study can be requested from the corresponding authors.

© 2025 The Author(s). Advanced Functional Materials published by Wiley-VCH GmbH

16163028, 2025, 26, Downloaded from https://advanced.onlinelibrary.wiley.com/doi/10.1002/adfm.202421537 by Koc University, Wiley Online Library on [02/09/2025]. See the Terms and Conditions (https://onlinelibrary.wiley.com/terms-and-conditions) on Wiley Online Library for rules of use; OA articles are governed by the applicable Creative Commons License

Keywords

antibacterial, bacteria, biomaterial infections, graphene quantum dots, photodynamic therapy (PDT), reactive oxygen species, singlet oxygen

Received: November 7, 2024
Revised: January 2, 2025
Published online: February 9, 2025

[1] *Nat. Rev. Microbiol.* **2024**, *22*, 589.
[2] S. Shivalkar, F. Arshad, A. K. Sahoo, Md. P. Sk, *ACS Omega* **2022**, *7*, 33358.
[3] Q. Yu, C. Wang, X. Zhang, H. Chen, M. X. Wu, M. Lu, *ACS Nano* **2024**, *18*, 14085.
[4] W. H. Organization, *Antimicrobial resistance: global report on surveillance*, WHO press, World Health Organization, Geneve **2014**, https://apps.who.int/iris/bitstream/10665/112642/1/9789241564748_eng.pdf.
[5] W. H. Organization, *Global antimicrobial resistance and use surveillance system (GLASS) report: 2021*, WHO press, World Health Organization, Geneve, **2021**, https://www.who.int/publications-detail-redirect/9789240027336.
[6] W. H. Organization, *WHO report on surveillance of antibiotic consumption: 2016–2018 early implementation:*, WHO press, World Health Organization, Geneve, **2018**, https://iris.who.int/bitstream/handle/10665/277359/9789241514880-eng.pdf
[7] T. Ali, S. Ahmed, M. Aslam, *Antibiotics* **2023**, *12*, 523.
[8] Y. Yu, L. Mei, Y. Shi, X. Zhang, K. Cheng, F. Cao, L. Zhang, J. Xu, X. Li, Z. Xu, *J. Mater. Chem. B* **2020**, *8*, 1371.
[9] A. de Breij, et al., *Sci. Transl. Med.* **2018**, *10*, eaan4044.
[10] M. Riool, et al., *Front. Chem.* **2017**, *5*, 63.
[11] J. Ghorbani, et al., *Laser Ther.* **2018**, *27*, 293.
[12] X. Pang, D. Li, J. Zhu, J. Cheng, G. Liu, *Nano-Micro Lett.* **2020**, *12*, 144.
[13] I. Lee, J. Moon, H. Lee, S. Koh, G.-M. Kim, L. Gauthé, F. Stellacci, Y. S. Huh, P. Kim, D. C. Lee, *Biomater. Sci.* **2022**, *10*, 7149.
[14] S. Wen, T. Wu, H. Long, L. Ke, S. Deng, L. Huang, J. Zhang, S. Tan, *ACS Appl. Mater. Interfaces* **2021**, *13*, 21979.
[15] S. U. Khan, et al., *Chem. Eng. J.* **2024**, *480*, 148140.
[16] Z. M. Markovic, D. D. Milivojevic, J. Kovac, B. M. Todorovic Markovic, *Polymers* **2024**, *16*, 1646.
[17] J. C. Ge, et al., *Nat. Commun.* **2014**, *5*, 4596.
[18] A. Halder, M. Godoy-Gallardo, J. Ashley, X. Feng, T. Zhou, L. Hosta-Rigau, Y. Sun, *ACS Appl. Bio Mater.* **2018**, *1*, 452.
[19] T. A. Tabish, C. J. Scotton, D. C. J Ferguson, L. Lin, A. V. der Veen, S. Lowry, M. Ali, F. Jabeen, M. Ali, P. G. Winyard, S. Zhang, *Nanomedicine* **2018**, *13*, 1923.
[20] G. Bae, H. Cho, B. H. Hong, *Nanotechnology* **2024**, *35*, 372001.
[21] L. Wang, Y. Wang, T. Xu, H. Liao, C. Yao, Y. Liu, Z. Li, Z. Chen, D. Pan, L. Sun, M. Wu, *Nat. Commun.* **2014**, *5*, 5357.
[22] N.-J. Kuo, Y.-S. Chen, C.-W. Wu, C.-Y. Huang, Y.-H. Chan, I-W. P. Chen, *Sci. Rep.* **2016**, *6*, 30426.
[23] H. Zhang, et al., *Nat. Commun.* **2024**, *15*, 2980.
[24] S. Chung, R. A. Revia, M. Zhang, *Adv. Mater.* **2021**, *33*, 1904362.
[25] X. T. Zheng, A. Ananthanarayanan, K. Q. Luo, P. Chen, *Small* **2015**, *11*, 1620.
[26] X. Yan, X. Cui, L. S. Li, *J. Am. Chem. Soc.* **2010**, *132*, 5944.
[27] T. Selvakumar, M. Rajaram, A. Natarajan, L. Harikrishnan, K. Alwar, A. Rajaram, *ACS Omega* **2022**, *7*, 12825
[28] R. Ye, C. Xiang, J. Lin, Z. Peng, K. Huang, Z. Yan, N. P. Cook, E. L. G. Samuel, C.-C. Hwang, G. Ruan, G. Ceriotti, A.-R. O. Raji, A. A. Martí, J. M. Tour, *Nat. Commun.* **2013**, *4*, 2943.
[29] K. Rajendiran, et al., *Polymers* **2019**, *11*, 1670.
[30] W.-S. Kuo, et al., *ACS Appl. Mater. Interfaces* **2018**, *10*, 14438.
[31] A. Kumar, M. I. Sayyed, D. Punina, E. Naranjo, E. Jácome, M. K. Abdulameer, H. J. Albazoni, Z. Shariatinia, *RSC Adv.* **2023**, *13*, 29163.
[32] H. Sun, N. Gao, K. Dong, J. Ren, X. Qu, *ACS Nano* **2014**, *8*, 6202.
[33] X. Tan, Y. Li, X. Li, S. Zhou, L. Fan, S. Yang, *Chem. Commun.* **2015**, *51*, 2544.
[34] Z. Li, D. Wang, M. Xu, J. Wang, X. Hu, S. Anwar, A. C. Tedesco, P. C. Morais, H. Bi, *J. Mater. Chem. B* **2020**, *8*, 2598.
[35] L. F. Wang, et al., *ACS Appl. Mater. Interfaces* **2019**, *11*, 21822.
[36] Y. Chong, C. Ge, G. Fang, X. Tian, X. Ma, T. Wen, W. G. Wamer, C. Chen, Z. Chai, J.-J. Yin, *ACS Nano* **2016**, *10*, 8690.
[37] W.-S. Kuo, H.-H. Chen, S.-Y. Chen, C.-Y. Chang, P.-C. Chen, Y.-I. Hou, Y.-T. Shao, H.-F. Kao, C.-L. Lilian Hsu, Y.-C. Chen, S.-J. Chen, S.-R. Wu, J.-Y. Wang, *Biomaterials* **2017**, *120*, 185.
[38] M. Milenkovic, G. Ciasca, A. Bonasera, M. Scopelliti, O. Markovic, T. Verbic, B. T. Markovic, S. Jovanovic, *J. Photochem. Photobiol., B* **2024**, *250*, 112818.
[39] C. W. K. Rosman, J. M. van Dijl, J. Sjollema, *Crit. Rev. Microbiol.* **2022**, *48*, 624.
[40] H. J. Busscher, H. C. van der Mei, G. Subbiahdoss, P. C. Jutte, J. J. A. M. van den Dungen, S. A. J. Zaat, M. J. Schultz, D. W. Grainger, *Sci. Transl. Med.* **2012**, *4*, 153rv10.
[41] L. Wang, Y. Wang, T. Xu, H. Liao, C. Yao, Y. Liu, Z. Li, Z. Chen, D. Pan, L. Sun, M. Wu, *Nat. Commun.* **2014**, *5*, 5357.
[42] J. Chen, A. Than, N. Li, A. Ananthanarayanan, X. Zheng, F. Xi, J. Liu, J. Tian, P. Chen, *FlatChem* **2017**, *5*, 25.
[43] D. Medina-Lopez, T. Liu, S. Osella, H. Levy-Falk, N. Rolland, C. Elias, G. Huber, P. Ticku, L. Rondin, B. Jousselme, D. Beljonne, J.-S. Lauret, S. Campidelli, *Nat. Commun.* **2023**, *14*, 4728.
[44] S. Dadwal, H. Deol, M. Kumar, V. Bhalla, *Sci. Rep.* **2019**, *9*, 11142.
[45] G. Feng, et al., *ACS Appl. Mater. Interfaces* **2016**, *8*, 21193.
[46] S. Xu, Y. Yuan, X. Cai, C.-J. Zhang, F. Hu, J. Liang, G. Zhang, D. Zhang, B. Liu, *Chem. Sci.* **2015**, *6*, 5824.
[47] Y. Zhang, C. Yang, D. Yang, Z. Shao, Y. Hu, J. Chen, L. Yuwen, L. Weng, Z. Luo, L. Wang, *Phys. Chem. Chem. Phys.* **2018**, *20*, 17262.
[48] C. Schweitzer, R. Schmidt, *Chem. Rev.* **2003**, *103*, 1685.
[49] C. M. Marian, *Wiley Interdiscip. Rev.: Comput. Mol. Sci.* **2012**, *2*, 187.
[50] P. K. Samanta, D. Kim, V. Coropceanu, J.-L. Brédas, *J. Am. Chem. Soc.* **2017**, *139*, 4042.
[51] H. J. Busscher, H. C. van der Mei, G. Subbiahdoss, P. C. Jutte, J. J. A. M. van den Dungen, S. A. J. Zaat, M J. Schultz, D. W. Grainger, *Sci. Transl. Med.* **2012**, *4*, 153rv10.
[52] J. Dong, W. Wang, W. Zhou, S. Zhang, M. Li, N. Li, G. Pan, X. Zhang, J. Bai, C. Zhu, *Biomater. Res.* **2022**, *26*, 72.
[53] J. J. Boelens, J. Dankert, J. L. Murk, J. J. Weening, T. van der Poll, K. P. Dingemans, L. Koole, J. D. Laman, S. A. J. Zaat, *J. Infect. Dis.* **2000**, *181*, 1337.
[54] M. Riool, L. de Boer, V. Jaspers, C. M. van der Loos, W. J. B. van Wamel, G. Wu, P. H. S. Kwakman, S. A. J. Zaat, *Acta Biomater.* **2014**, *10*, 5202.
[55] R. K. Sen, N. Murthy, S. S. Gill, O. N. Nagi, *J. Orthop. Surg.* **2000**, *8*, 1.
[56] C. Guarch-Pérez, M. Riool, L. de Boer, P. Kloen, S. A. J. Zaat, *J. Hosp. Infect.* **2023**, *140*, 62.
[57] S. Nizamoglu, M. C. Gather, M. Humar, M. Choi, S. Kim, K. S. Kim, S. K. Hahn, G. Scarcelli, M. Randolph, R. W. Redmond, S. H. Yun, *Nat. Commun.* **2016**, *7*, 10374.

© 2025 The Author(s). Advanced Functional Materials published by Wiley-VCH GmbH

16163028, 2025, 26, Downloaded from https://advanced.onlinelibrary.wiley.com/doi/10.1002/adfm.202421537 by Koc University, Wiley Online Library on [02/09/2025]. See the Terms and Conditions (https://onlinelibrary.wiley.com/terms-and-conditions) on Wiley Online Library for rules of use; OA articles are governed by the applicable Creative Commons License